MIXED MODE FRACTURE IN REINFORCED CONCRETE WITH LOW VOLUME FRACTION OF STEEL FIBERS

M.T. Kazemi* and I. Zakeri

Department of Civil Engineering, Sharif University of Technology
P.O. Box 11365-9313, Tehran, Iran
kazemi@sharif.edu - zakeri@civil.sharif.edu - iman_zakery@yahoo.com

F. Vossoughi Shahvari

Department of Civil Engineering, University of California Berkeley
CA94720 California, U.S.A.
vosoughi@ce.berkeley.edu -fvosoughi@gmail.com

*Corresponding Author

(Received: April 21, 2009 – Accepted in Revised Form: October 5, 2009)

Abstract An investigation into the mixed mode fracture of steel fiber reinforced concrete (SFRC) beams with one percent volume fraction of steel fiber is presented. A series of notched beams with different notch depths and locations are tested under three-point bending. The test results for apparent fracture toughness, crack trajectories, and fracture energy are presented. The crack paths for SFRC and plain concrete beams are compared. The apparent fracture toughness values were more scattered for SFRC than for plain concrete. The load-deflection curves were used to obtain the fracture energy. To this end, two methods were utilized for center notched beams, and the results were comparable to each other. It is observed that fracture energy is a more reliable material property than apparent fracture toughness, and its scatter is less.

Keywords Steel Fiber Reinforced Concrete, Stress Intensity Factor, Mixed Mode, Fracture Energy, Crack Trajectory

چکیده تحقیق و بررسی مد مرکب شکست تیر ساخته شده با بتن با فیبرهای فولادی که دارای یک درصد حجم فیبر فولادی می‌باشند، ارائه شده است. مجموعه‌ای از تیرها که در آنها شکافی با عمق‌های مختلف و محل‌های متفاوت ایجاد شده است، تحت آزمایش خمش سه‌نقطه قرار گرفته‌اند. نتایج آزمایش‌ها از قبیل انرژی شکست، توزیع ترک‌ها و طاقت شکست ارائه شده است. مسیر ترک‌ها در بتن با فیبرهای فولادی و بتن معمولی مورد مقایشه قرار گرفته است. پراکندگی مقادیر طاقت شکست برای بتن با فیبرهای فولادی بسیار گسترده‌تر از بتن معمولی است. نمودارهای بار–تغییرشکل نیز برای یافتن انرژی شکست مورد استفاده قرار گرفته است. دو روش برای تیرهایی که فاقی در وسط دارند مورد استفاده قرار گرفته و نتایج با یکدیگر مقایسه گردید. مشاهده گردید که انرژی شکست خاصیت قابل اعتمادتری نسبت به طاقت شکست می‌باشد و پراکندگی بسیار کمتری دارد.

1. INTRODUCTION

Concrete is a brittle material with low tensile strength and low strain capacity, that result in low resistance to cracking. To improve such properties, fiber reinforced concrete (FRC) has been developed. Fibers are intended to improve tensile strength, flexural strength, toughness and impact strength, to change failure mode by means of improving post-cracking ductility, and to control cracking [1-3]. Fibers bridging crack faces restrict the cracks from widening and propagating, and thus impart "toughness" or energy absorption capacity to the composite. Toughness Measurment have received considerable attention during the last thirty years as a means of characterizing the energy absorption properties of FRC. The main energy consumption factors in the presence of fibers are fiber-matrix interface debonding, fiber fracture, fiber pullout, and shear yielding of the fibers. Depending on fiber length, orientation towards crack plane and anchorage condition in concrete, the fibers are either pulled out or tensile fracture occurs. The fracture of cementitious composite

materials is typified by the presence of a fracture process zone (FPZ) in which many kinds of micro-failure mechanisms take place [4-7].

Fiber reinforced concrete has been widely used in infrastructure where tensile cracks may occur. FRC have many application such as the construction of airport and highway, industrial floor, bridge deck and earthquake resistance construction. Generally, the fiber volume fraction in FRC are in the range of 0.5 % to 1.5 %, and it is refferd to low volume fraction of fiber.

Linear elastic fracture mechanics (LEFM) is valid when the fracture process zone (FPZ) is small, which is not the case for laboratory sized concrete specimens. Consequently, different nonlinear models have been proposed. The fracture of FRC is more complicated than that of plain concrete. These materials are characterized by the development of fiber bridging zone (FBZ) in the wake of the continuous tip of the matrix crack and matrix FPZ [8-11]. Soroushian, et al [12] performed an experimental program on notched beams of fiber reinforced concrete with different notch depths and locations and concluded that, due to the significant influence of fibers on the post-peak behavior of concrete, nonlinear fracture mechanics principles are more applicable.

Mode-I fracture is a clear type of crack propagation in fiber reinforced concrete. Mode-II and III are complex failure modes. In these modes the stress normal to the crack surface needs to be approximately zero and only in-plane shear stress should exist. Even when these conditions can be realized, a combination of different stresses exist (shear, tension, compression and bending) over the crack surface. In practice most cracks in fiber reinforced concrete result from mode-I fracture, or from the combination of mode-I and other modes. A frequently observed combination of modes is the combination of mode-I and mode-II, the so-called mixed-mode fracture. Typical examples are diagonal shear failure of fiber reinforced concrete beams or punching of flat slabs.

The purpose of this research was to further study, experimentally, the mixed mode fracture of low volume fraction SFRC and compare some of its characteristics with those of plain concrete. Apparent fracture toughness, crack initiation angle and trajectory, and fracture energy were obtained from the test results.

1.1. Mixed Mode Cracking Based on linear elasticity, if a crack is loaded in combined mode I and II, the stress components σ_θ and $\tau_{r\theta}$ (Figure 1) near the tip of the crack can be obtained by adding the stresses due to mode I and mode II [5,13]:

$$\sigma_\theta = \frac{1}{\sqrt{2\pi r}}\cos\frac{\theta}{2}[K_I\cos^2\frac{\theta}{2} - \frac{3}{2}K_{II}\sin\theta] \quad (1)$$

$$\tau_{r\theta} = \frac{1}{2\sqrt{2\pi r}}\cos\frac{\theta}{2}[K_I\sin\theta + K_{II}(3\cos\theta - 1)] \quad (2)$$

Where K_I and K_{II} are stress intensity factors for mode I and mode II fracture, respectively. As in mode I fracture, where quasi-static crack growth requires that $K_I = K_{IC}$, for the in-plane mixed mode problems, the straight phenomenological approach involves postulating that fracture may initiate when the values of K_I and K_{II} meet a certain critical condition.

The most commonly used criterion is based on the near-tip stress distribution (maximum principal stress) [5,13,14]. This criterion states that, for in-plane mixed mode, crack growth will happen perpendicular to the direction of maximum principal stress. The maximum of σ_θ Figure 1, happens when $\tau_{r\theta}$ is zero and consequently from Equation 2, the initiation angle, θ_m, is given by:

$$\tan\frac{\theta_m}{2} = \frac{K_I}{4K_{II}}(1 \pm \sqrt{1 + \frac{8K_{II}^2}{K_I^2}}) \quad (3)$$

In an alternative approach, for composite materials fracture energy, G_F, is introduced. G_F is a measure of the energy that needs to be spent to generate a unit surface crack [13]. The approximate fracture energy is calculated as:

$$G_F = \frac{W_F\cos\theta}{t(b-a_0)} \quad (4)$$

Where W_F is the total work needed to break the beam specimen; t, b, a_0, and θ are thickness, beam depth, notch depth, and crack angle respectively. Fracture energy is one of the parameters used in the cohesive models, proven a useful tool to analyze mixed mode fracture, too.

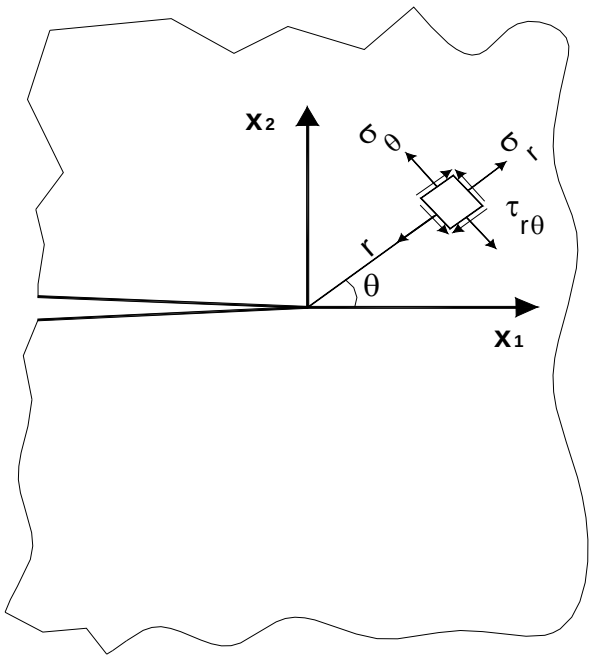

Figure 1. Axes for near crack tip field description.

1.2. Experimantal Program Three point bend notched beam tests with notches at different off-set ratios, $\gamma = 2x/S$, were performed (Figure 2). The length, depth, and thickness of the specimens were, L = 700 mm, b = 150 mm, and t = 150 mm, respectively. In addition, the nominal span of all the beams was S = 600 mm. In each position of the notch, three different notch depths were tested. Thus, the variables for all the tests were the distance between the centerline of the beam and the place of notch, x, and the notch depth, a_0.

Four different off-set ratios ranging from 0 to 0.6 by an increment of 0.2, and each with various notch to depth ratio, $\alpha = a_0/b$, from 0.2 to 0.6 with 0.2 steps were used in this study. In each notch configuration two specimens were cast, so a total of 24 beam specimens were cast to account for different off-set ratios and notch depths. Two extra beams were cast without any notch. In addition, control cylinders of 152 mm × 305 mm were cast to measure the compressive strength.

Six batches with a single mixture were used to cast the specimens. A mould with four compartments was used for the casting. The notches for specimens were produced by placing paper plates with 1.5 mm thickness and different depths in the top side of mould before casting. The basic mix ingredients were type II Portland cement, crushed coarse aggregate, sand, water, steel fibers and superplasticizer. The fiber content of concrete was 1% by volume. Mixture proportioning was in accordance with ACI 544 recommendation [15]. The maximum size of coarse aggregate was 12.5 mm, and both coarse aggregate and sand were utilized in saturated surface dry (SSD) condition. Due to the absence of larger coarse aggregate content, and utilization of fibers, a superplasticizer was used and the mixing time was increased to attain the required workability without segregation. The weight ratios of water, coarse aggregate, sand, steel fibers and superplasticizer to cement were 0.45, 2, 2.5, 0.195 and 0.005, respectively. Steel fibers were crimped (Figure 3) and had a tensile strength of 600 MPa, and their modulus of elasticity was 200 GPa. The testing age was almost 45 days for all the specimens.

2. CALCULATION OF STRESS INTENSITY FACTORS

A finite element code was used to calculate the stress intensity factors for different notch

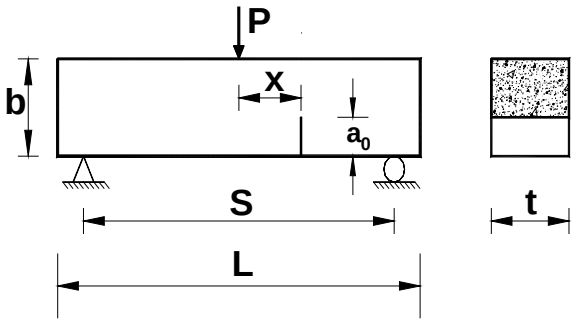

Figure 2. Schematic view of mixed mode beam specimens.

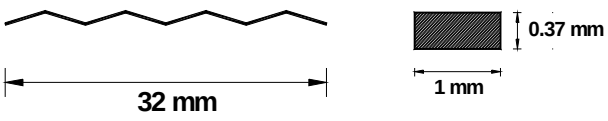

Figure 3. Geometry of steel fibers.

configurations. The values of K_I and K_{II} were calculated from the nodal displacements near the crack tip. The stress intensity factor is expressed as $K = \sigma\sqrt{\pi a}\, f(\alpha,\gamma)$, where $\sigma = a$ stress measure, $\alpha = a/b$ and a = crack length. Since there were two stress intensity factors for mode I and mode II, i.e., K_I and K_{II}, so functions f_I and f_{II} were evaluated for each crack configuration. The stress intensity factors may be sought as:

$$K_I = \sigma_N \sqrt{b}\sqrt{\pi\alpha}\, f_I(\alpha,\gamma) \quad (5)$$

$$K_{II} = \tau_N \sqrt{b}\sqrt{\pi\alpha}\, f_{II}(\alpha,\gamma) \quad (6)$$

Where:

$$\sigma_N = \frac{6M}{b^2 t(1-\alpha)^2} \quad (7)$$

$$\tau_N = \frac{V}{bt(1-\alpha)} \quad (8)$$

$$M = \frac{P}{4}(S-2x) + \frac{wL}{4}(S-2x) - \frac{w}{8}(L-2x)^2 \quad (9)$$

$$V = \frac{P}{2} + wx \quad (10)$$

Where $0 < x < S/2$, w = weight per unit length of the beam; $f_I(\alpha,\gamma)$ and $f_{II}(\alpha,\gamma)$ are dimensionless functions, M = bending moment at distance $x = \gamma S/2$ from the centerline, and V = shear force at distance x. The factor $(1-\alpha)$ was also entered to account for the net area of the beam section. By analyzing a notched beam with different notch configurations under assumed point load, P, and using Equations 5 to 10, dimensionless functions, f_I and f_{II}, were calculated for required values of α and γ [5,13]. The results for f_I and f_{II} are presented in Table 1.

Equations 5 to 10 with the appropriate values of f_I and f_{II}, which were calculated based on the point load P, could be used to calculate K_I and K_{II}, for any load. Hence, K_{ICM} and K_{IICM}, which are conventional critical stress intensity factors or apparent fracture toughnesses in the mixed mode condition for mode I and mode II, respectively, were obtained, based on measured failure load and weight of the beam. The results are based on LEFM data reduction even though the specimens are experiencing nonlinear condition.

TABLE 1. Dimensionless Functions for Stress Intensity Factors.

g = 2x/S	a = a_0/b	f_I	f_{II}
0.0	0.2	0.626	0.000
	0.4	0.422	0.000
	0.6	0.292	0.000
0.2	0.2	0.689	0.530
	0.4	0.459	0.671
	0.6	0.308	0.615
0.4	0.2	0.686	0.583
	0.4	0.457	0.729
	0.6	0.307	0.631
0.6	0.2	0.686	0.536
	0.4	0.457	0.693
	0.6	0.307	0.616

3. EVALUATION OF FRACTURE ENERGY

The self-weight of the beam and the energy not measured in the far end of the load-displacement of the test must be properly taken into account. To account for beam self-weight, amount of $P_0 = 4M_0/S$ should be added to the applied load, where M_0 = moment of the beam weight. The total work of fracture for center-notch specimens, $\gamma = 0$, is evaluated as [16,17]:

$$W_F = W_0 + 2P_0 u_0 \quad (11)$$

Where W_0 = the work done by applied load and u_0 = the recorded maximum displacement, when the recorded load becomes zero. Fracture energy may be obtained from Equation 4 with $\theta = 0$. In Figure 4, some typical total load-displacement curves are shown. To calculate the area between the curves, the curves of various beams are shifted to account for the beam self-weight. It is postulated

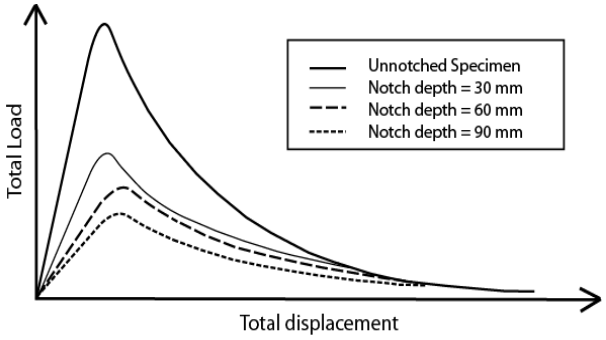

Figure 4. Theoretical total load-displacement curves for beams based on cohesive crack model.

that, for cohesive materials, the energy dissipates just on the fracture surface. Therefore, the total load-displacement curves should intersect asymptotically, and become tangent to each other. This fact enables us to get rid of the problems in considering the energy dissipated in the far end of the test [18].

In practice, this tangency of the curves is satisfied, but approximately. In this study, fracture energy values were also calculated by a second method, for center notched specimens, as:

$$G_F = \frac{\Delta W_F}{t\Delta a} \quad (12)$$

Where ΔW_F = area between load-displacement curves corresponding to two beams with notch length of a_0 and $a_0 + \Delta a$ and Δa is the difference between the initial notch depths for the two specimens.

3.1. Test Results For the sake of brevity; to each specimen a unit code was designated. The code is a four-digit number, which follows the F letter, standing for FRC. The first two digits show the distance (cm) between the loading point and the initial notch, the third digit indicates the notch depth (cm) and since for each notch configuration two specimens were cast, the last digit is added to differentiate these two, which takes the value of 1 or 2.

For the test reported here, the average compressive strength (f'_c) of SFRC was 32 MPa after 45 days. Furthermore, the average specific weight for all the batches was 2300 kg/m^3. Two specimens with α = 0.6 and γ = 0.2 ($a_0 = 90\,\text{mm}, x = 60\,\text{mm}$) did not have a good quality of concrete mix, so their results are not consistent with other specimens. Figure 5 shows the experimental records of load P vs. mid-span deflection for different initial notch depths and offsets. The initial part of these curves was corrected for extraneous initial displacements using the method described in ASTM C1018 [19]. In addition, the curves were corrected based on the results of elastic finite element analysis of the specimens with appropriate modulus of elasticity, by adjusting ascending part of experimental curve with the analytical one. Consequently, the post peak records of displacement (for each load) were changed in accordance to the displacement correction in the elastic part for the same amount of load. It should be mentioned that these corrections only change the evaluated W_F slightly, and its effect on other calculated parameters is negligible. The initial portion of load-deflection curves is shown more accurately to observe the effect of notch depth on the initial stiffness and softening slope. The curves are characterized by a sharp peak and a pronounced longer post peak area in comparison to plain concrete [5,20]. The results for measured peak loads, apparent fracture toughnesses and fracture energy which were calculated from the maximum load and the beam weight are listed in Table 2.

Figures 6 and 7, depict the variations of apparent fracture toughnesses in the mixed mode condition for mode I and mode II, i.e. K_{ICM} and K_{IICM}, for different notch-depth ratios, α, and offset ratios, γ. It can be observed that for each particular notch-depth ratio, as the offset ratio increases the value of K_{IICM} increases too.

In LEFM condition, a simple interaction relation for the failure locus based on values of K_I, K_{II} is proposed [5,13]:

$$\left(\frac{K_{ICM}}{K_{IC}}\right)^2 + \left(\frac{K_{IICM}}{K_{IIC}}\right)^2 = 1 \quad (13)$$

Where, K_{IC} and K_{IIC} are fracture toughness values for pure mode I and mode II, respectively. However, in FRC, due to the presence of large FPZ and FBZ, LEFM criteria are not suitable. In this study, by using a larger thickness (t=150mm), which results in smaller FPZ in comparison to other experiments, the plane strain condition was

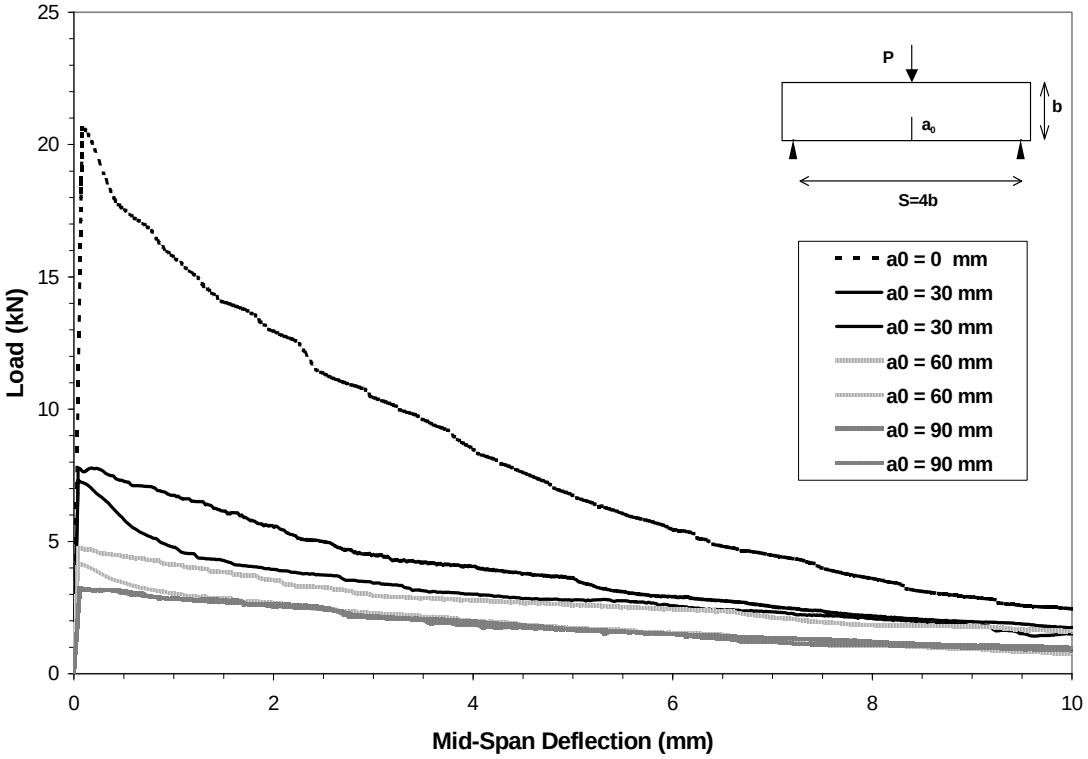
Load (kN)
Mid-Span Deflection (mm)
P
b
a_0
S=4b
a0 = 0 mm
a0 = 30 mm
a0 = 30 mm
a0 = 60 mm
a0 = 60 mm
a0 = 90 mm
a0 = 90 mm

(a)

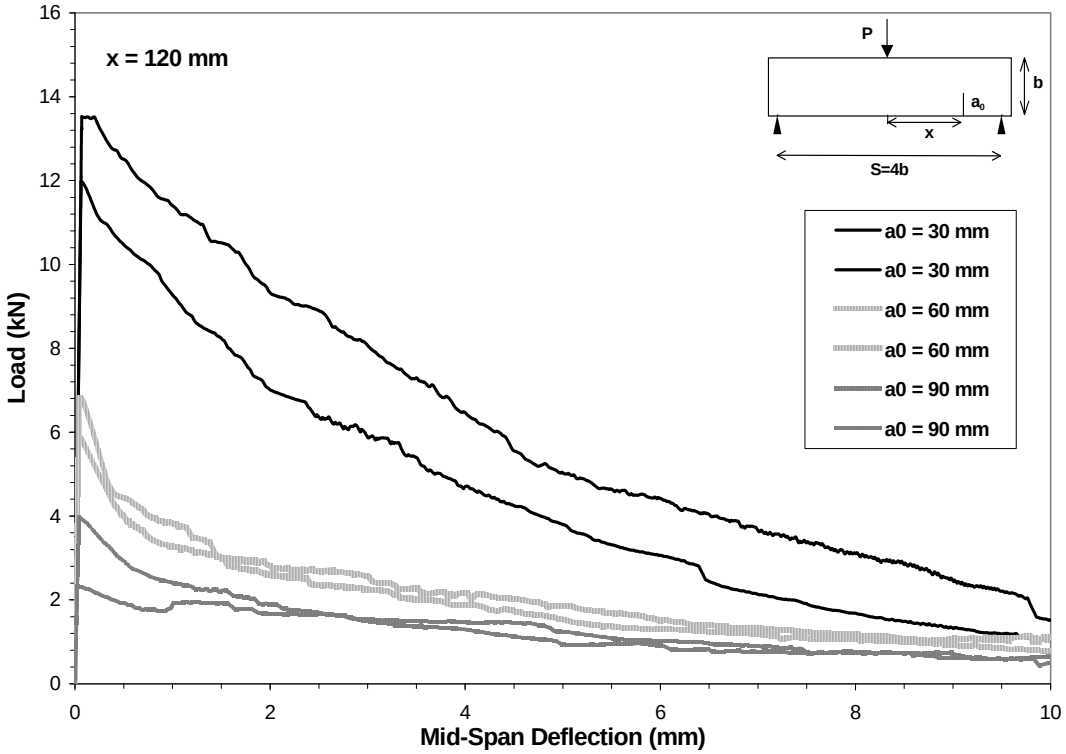
x = 120 mm
Load (kN)
Mid-Span Deflection (mm)
P
b
a_0
x
S=4b
a0 = 30 mm
a0 = 30 mm
a0 = 60 mm
a0 = 60 mm
a0 = 90 mm
a0 = 90 mm

(b)

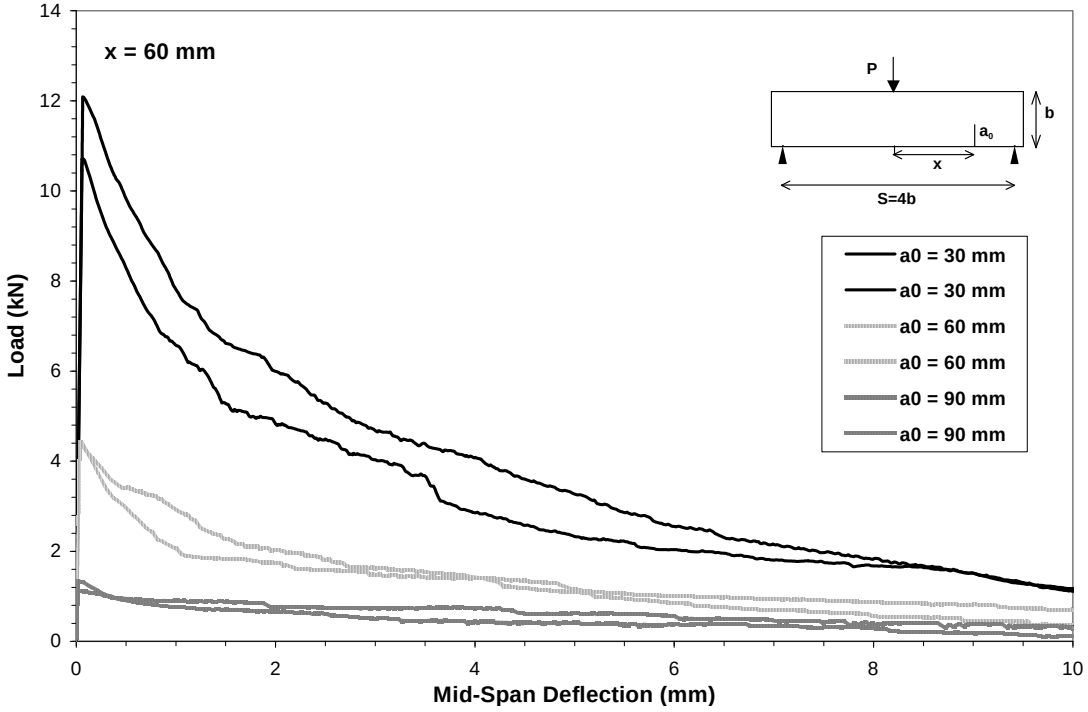

(c)

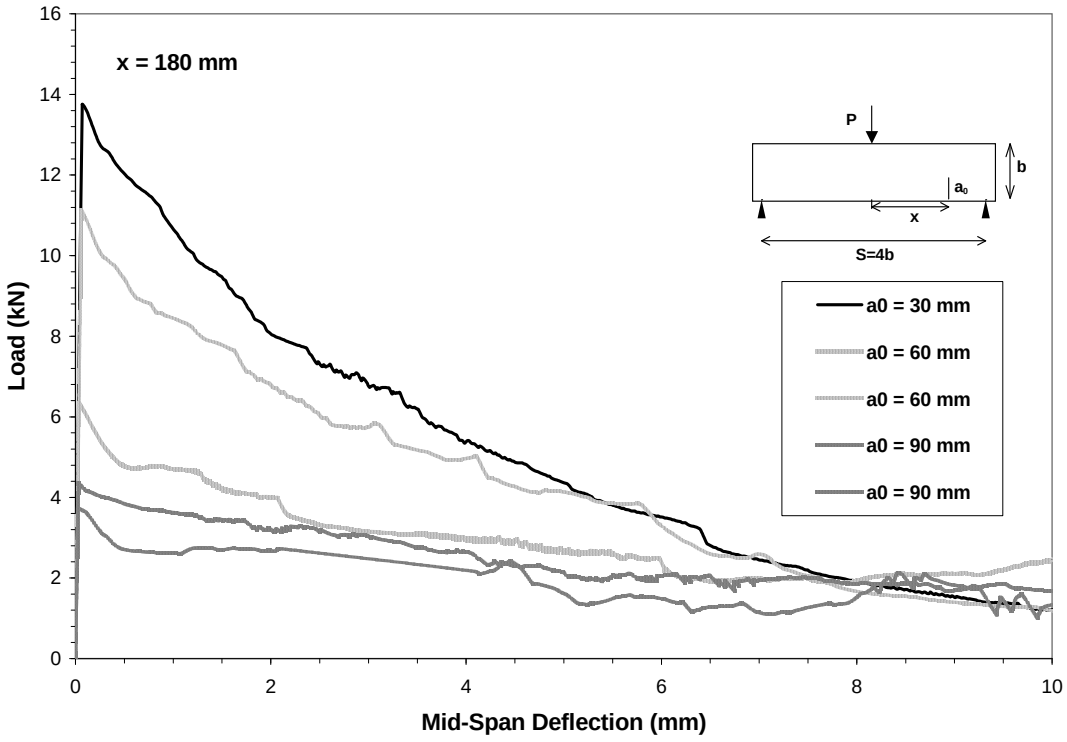

(d)

Figure 5. Load-deflection plots for different notch offsets and depths: (a) x = 0 mm (mode I), (b) x = 60 mm, (c) x = 120 mm and (d) x = 180 mm.

TABLE 2. Experimental Results of Peak Load, Apparent Mode I and II Fracture Toughnesses and Fracture Energy.

Specimen	x (mm)	a_0 (mm)	P_{max} (kN)	K_{ICM} (MPa.$m^{1/2}$)	K_{IICM} (MPa.$m^{1/2}$)	W_F (J)	R_1	R_2	G_F (kJ/m^2)
F0001	-	0.0	20.627	-	-	104.51	0.081	0.016	4.64
F0002	-	0.0	-	-	-	-	-	-	-
F0031	0	33.3	7.784	0.678	0.000	51.45	0.128	0.006	2.93
F0032	0	34.9	7.321	0.657	0.000	45.30	0.166	0.007	2.63
F0061	0	63.2	4.139	0.626	0.000	29.85	0.235	0.006	2.29
F0062	0	60.0	4.749	0.666	0.000	45.75	0.171	0.004	3.38
F0091	0	88.7	3.254	0.855	0.000	31.06	0.230	0.006	3.37
F0092	0	91.2	3.218	0.909	0.000	29.12	0.241	0.007	3.30
F0631	60	30.0	12.089	0.865	0.055	53.80	0.157	0.015	3.26
F0632	60	31.1	10.717	0.785	0.051	44.30	0.148	0.014	2.67
F0661	60	60.0	4.426	0.544	0.048	25.20	0.293	0.006	1.88
F0662	60	62.1	4.374	0.562	0.050	20.70	0.271	0.007	1.58
F0691	60	90.0	1.338	0.331	0.025	9.02	0.461	0.003	1.02
F0692	60	90.0	1.123	0.284	0.022	11.26	0.385	0.002	1.27
F1231	120	30.0	13.530	0.723	0.068	76.2	0.108	0.012	4.78
F1232	120	31.3	11.981	0.658	0.064	59.20	0.131	0.012	3.56
F1261	120	60.0	5.886	0.538	0.070	32.54	0.262	0.007	2.58
F1262	120	60.0	6.816	0.620	0.081	33.90	0.197	0.009	2.58
F1291	120	92.7	2.326	0.453	0.047	24.36	0.300	0.002	2.84
F1292	120	91.0	3.964	0.705	0.077	25.99	0.328	0.007	3.16
F1831	180	30.0	Failed	-	-	-	-	-	-
F1832	180	30.0	13.750	0.491	0.064	66.78	0.117	0.014	4.08
F1861	180	60.0	6.333	0.386	0.073	50.34	0.163	0.004	3.80
F1862	180	61.7	11.121	0.692	0.130	61.92	0.136	0.011	5.14
F1891	180	90.0	3.727	0.431	0.071	35.82	0.155	0.003	4.11
F1892	180	90.0	4.353	0.499	0.083	37.15	0.188	0.004	4.18

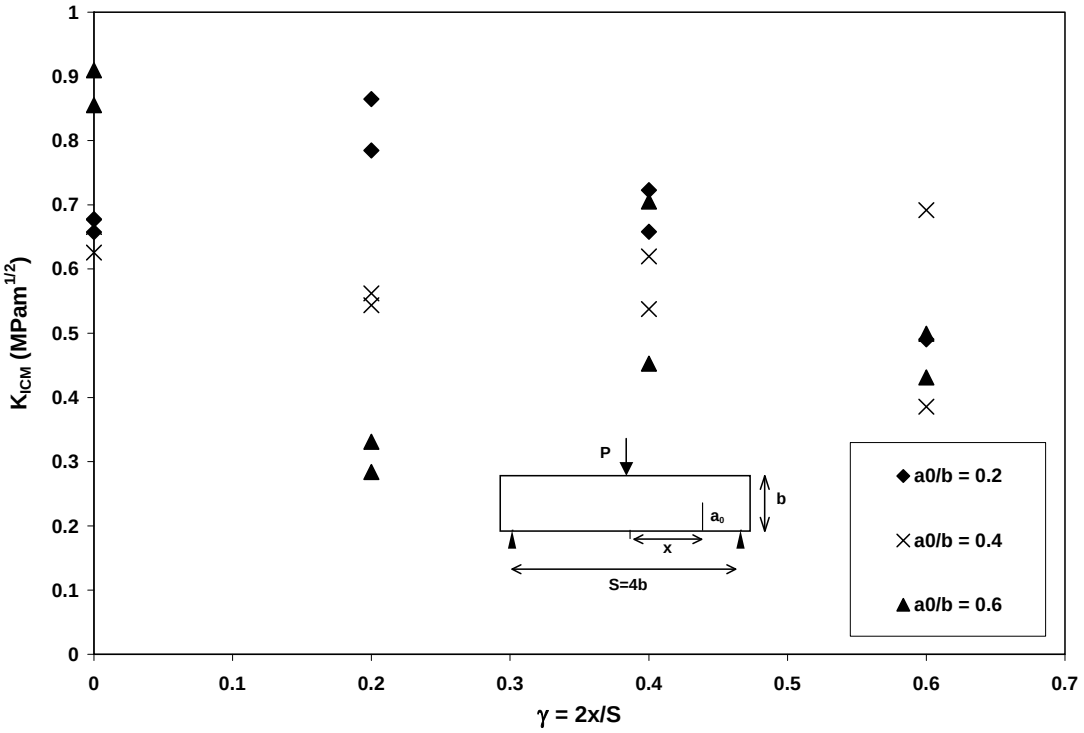

Figure 6. Apparent mode I fracture toughness for different notch configurations.

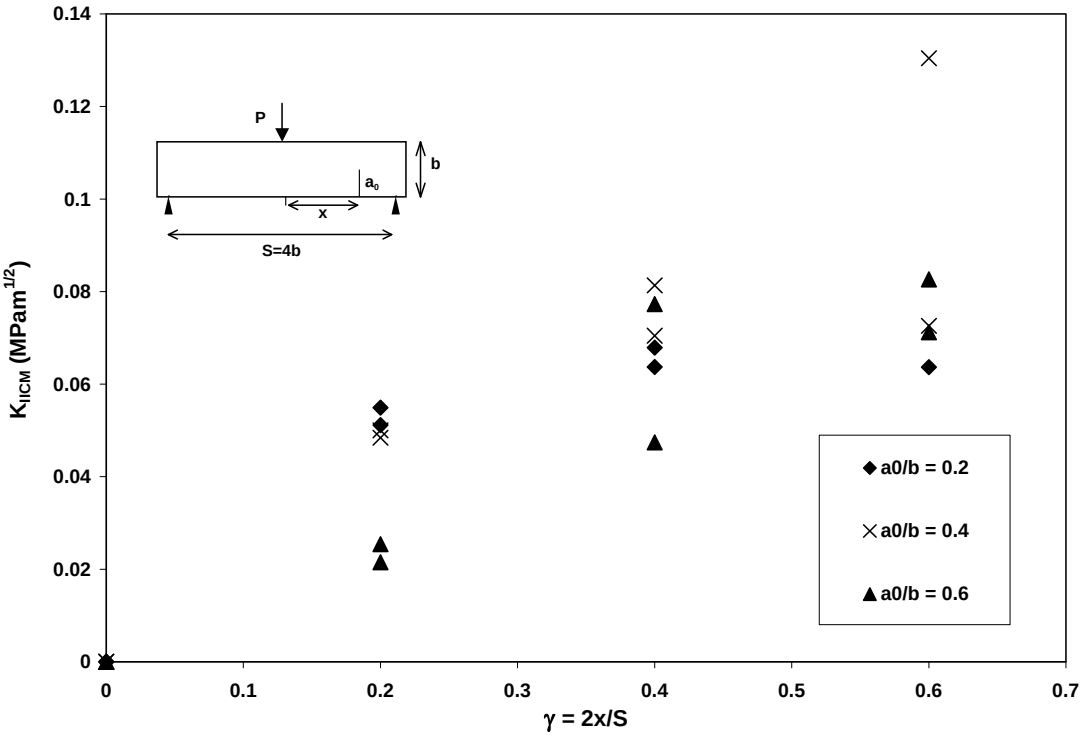

Figure 7. Apparent mode II fracture toughness for different notch configurations.

better approximated. Wollrab, et al [21] have investigated the effect of thickness on fracture behavior of plain concrete, and have concluded that fracture toughness decreases with increasing specimen thickness. The apparent mixed mode fracture toughness [5] is defined as:

$$K_C = \sqrt{\left(K_{ICM}\right)^2 + \left(K_{IICM}\right)^2} \quad (14)$$

Figure 8 shows the values of K_C for different notch configurations. The variation of K_C is scattered but it is almost independent of γ.

3.2. Crack Angle and Trajectories For each specimen, two angles were determined, the first was the initiation angle and the other was the final failure angle, which was calculated based on the intersection point of the crack with the beam's top side [5]. The initiation and final angles are reported for any of two specimens with the same notch location and depth in a separate adjacent column in the Table 3. Table 4 present the initiation and final angles for plain concrete. Some specimens have shown failures along nonorthogonal planes to the lateral sides of the beam, owing to non-planar deformations at the crack front, therefore the average angle through the thickness of the beam was considered. Figures 9 and 10 present the results for the crack angles in comparison to the theoretical results based on the maximum principal stress criterion for isotropic material, Equation 3. It is observed that the experimental values show a large scatter. This is mainly due to presence of fibers, which easily affect the crack angle in SFRC beam (compare Tables 3 and 4). The final failure angle was considered as the crack angle in the fracture energy calculations, since the difference between these angles was less for beams with same initial notch configurations.

Figure 11 shows the crack trajectories. For any of two specimens with the same notch location and depth, both sides are considered and for any notch, four trajectories are shown. The undulations in the crack path, which is not normally observed in metal fracture specimens, are caused by the aggregate and fibers dispersion. For the same reason, a difference of about one coarse aggregate

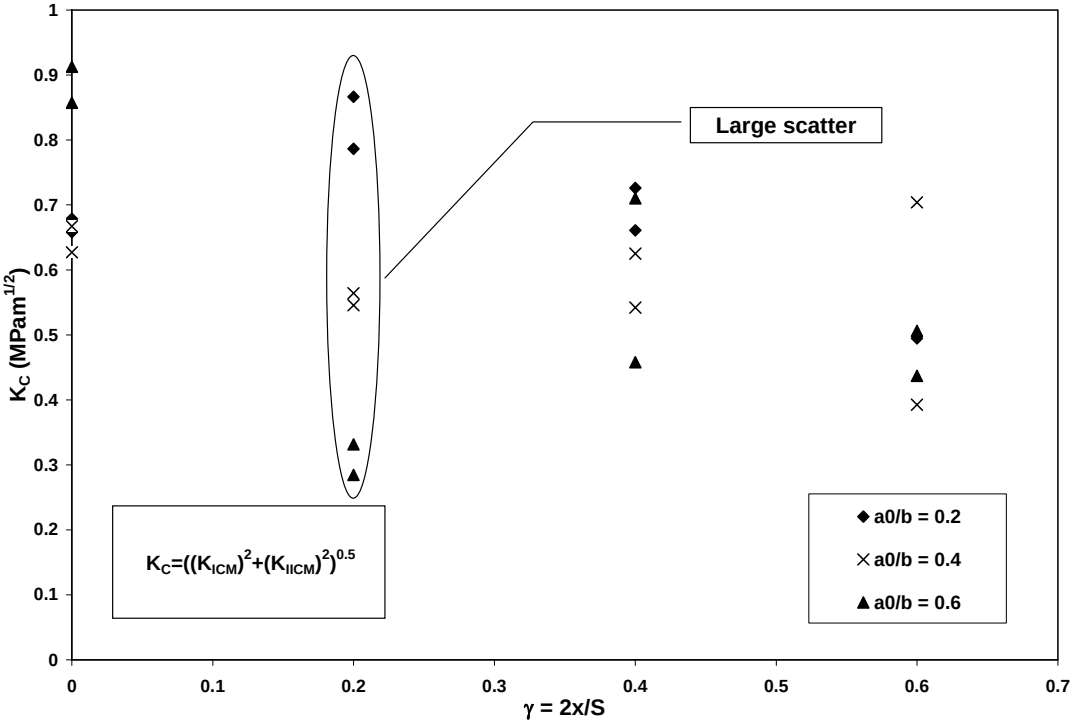

Figure 8. Variation of apparent mixed mode fracture toughness, K_C, for different notch configurations.

TABLE 3. Measured Initiation and Final Failure Angles for SFRC Specimens (Degree).

g = 2x/S	a_0/b	Initiation Angle		Final Angle	
0.0	0.2	5	5	0	0
	0.4	0	6	0	0
	0.6	0	0	0	0
0.2	0.2	22	14	24	22
	0.4	11	15	8	5
	0.6	9	10	8	10
0.4	0.2	25	14	27	21
	0.4	14	13	21	14
	0.6	12	26	5	22
0.6	0.2	-	22	-	25
	0.4	14	29	12	25
	0.6	10	14	15	10

TABLE 4. Measured Initiation and Final Failure Angles for Plain Concrete (Degree) (Kazemi, et al [20]).

g = 2x/S	a_0/b	Initiation Angle		Final Angle	
0.0	0.2	0	0	0	0
	0.4	0	0	0	0
	0.6	0	0	0	0
0.2	0.2	5	8	8	8
	0.4	10	17	13	10
	0.6	20	-	14	-
0.4	0.2	11	21	11	23
	0.4	13	18	13	8
	0.6	34	30	12	-
0.6	0.2	-	-	-	22
	0.4	22	25	26	19
	0.6	36	31	30	30

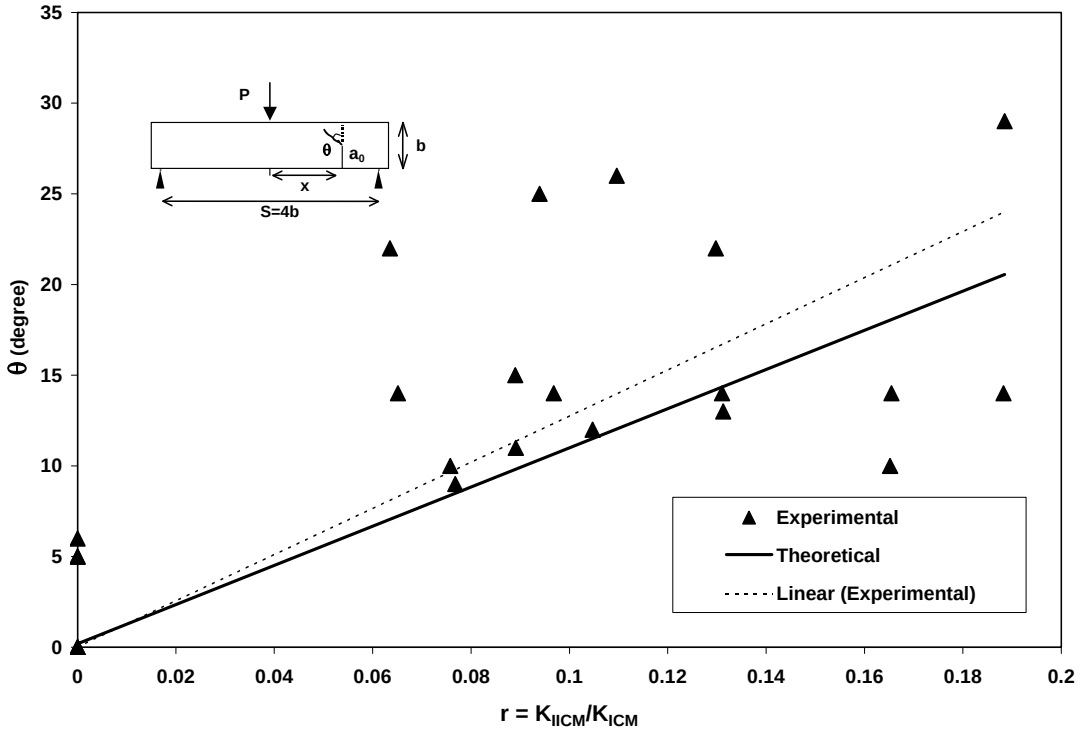

Figure 9. Theoretical prediction and experimental measurements of initiation angle.

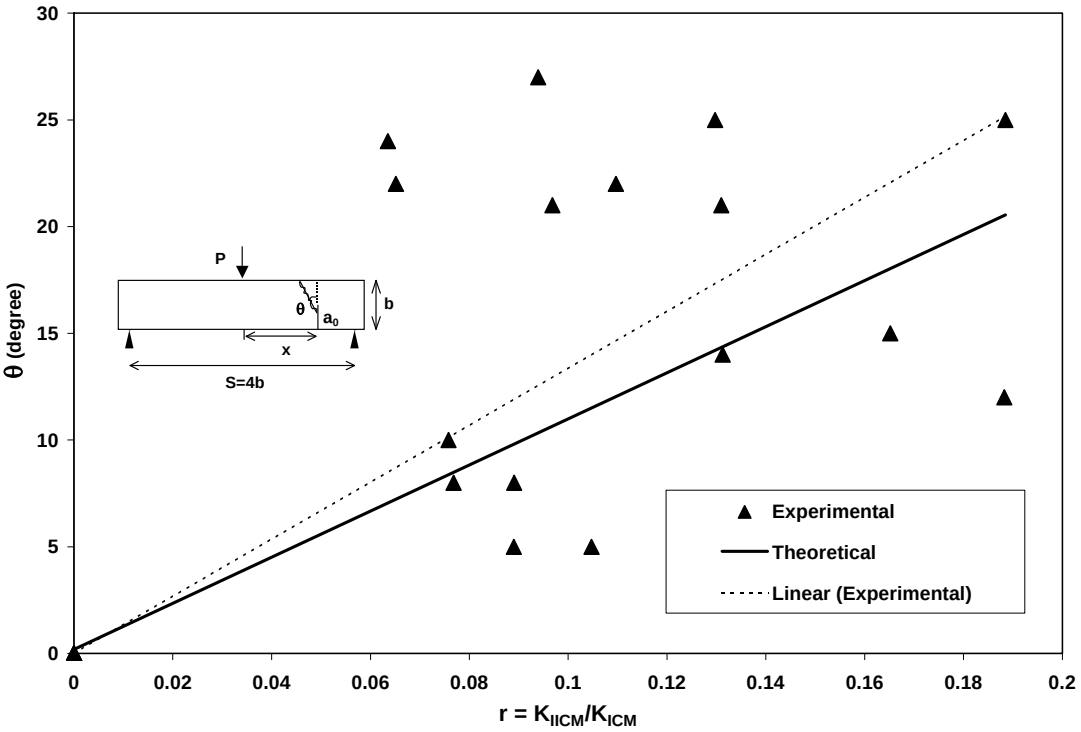

Figure 10. Theoretical prediction and experimental measurements of final failure angle.

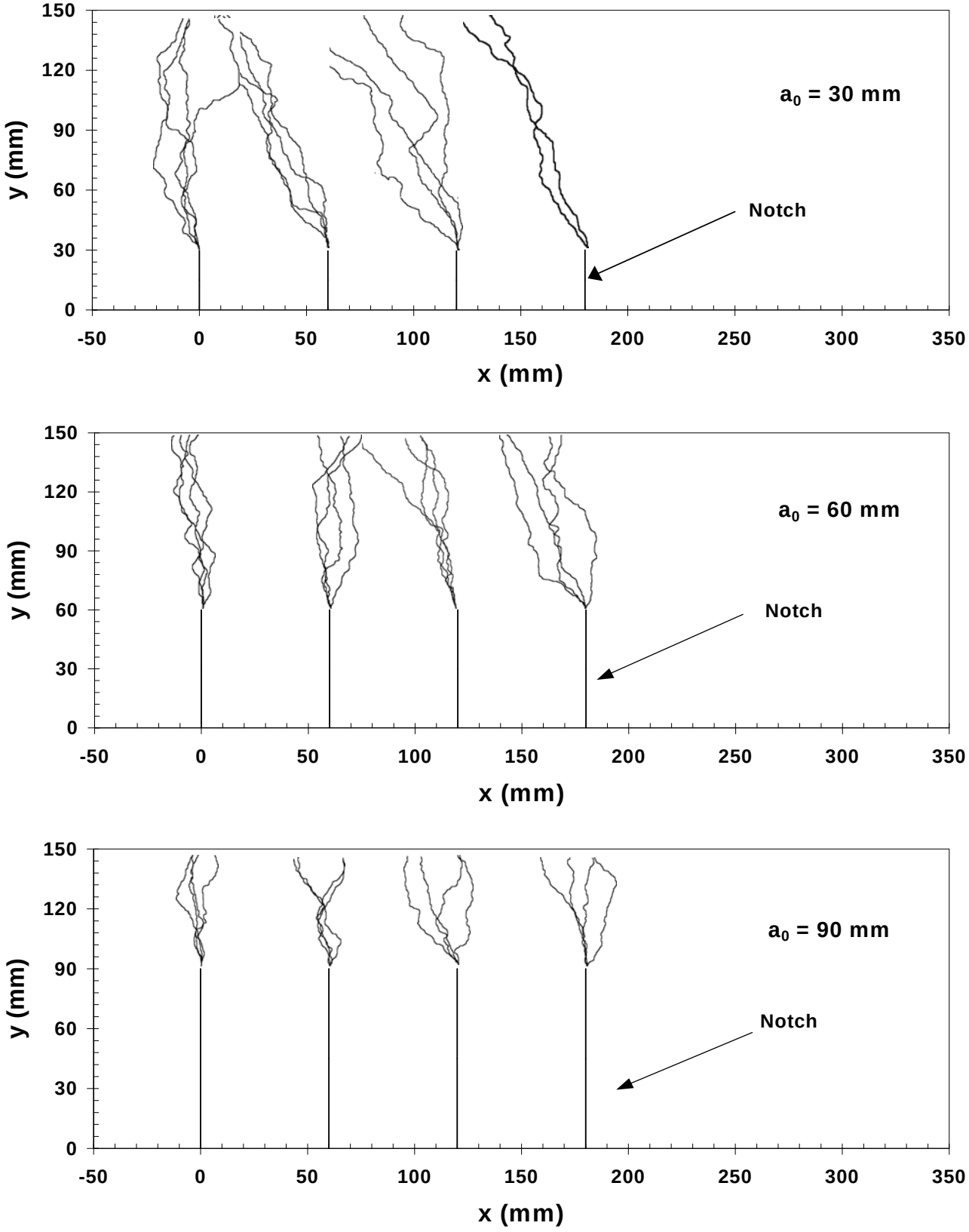

Figure 11. Crack trajectories for SFRC specimens.

size was observed between the crack paths on the front and the back surface of each specimen. In the case of lower notch depths, the crack path seems better predictable. This is because in those specimens the ligament size is large enough, with compare to maximum aggregate size, for the crack to correct its path as it is for the homogeneous materials. The crack patterns reveal that, by increasing the offset ratio the final failure angle of the crack increases, which highlights the effect of mode II in fracture. Figure 12 shows the crack trajectories for plain concrete. As can be seen from Figures 11 and 12, the crack paths for SFRC show more scatter for each crack configuration when compared to the plain concrete. A qualitative judgment with the naked eye indicated that on the fracture surfaces in all specimens the fiber pull-out mechanism was dominant. In addition, some spalling was present.

3.3. Fracture Energy The results for fracture energy are shown in Table 2 and Figure 13. To obtain these, W_F values were calculated for each specimen.

These values were evaluated, using Equations 4 and 11, by calculating the area under load-deflection curve and then adding the work of weight. In Table 2, the ratios of work of weight, $W_W = 2P_0u_0$, to total work, W_F, are shown ($R_1 = W_W/W_F$). The average was 0.211 for our study. This ratio can be more significant for larger specimens [22]. In addition, the ratio of work up to the peak load, W_{Pmax}, to W_F is shown as R_2, which, with small amounts, emphasizes the significant effect of fibers in the energy absorption. For plain concrete, G_F is considered as a material property, i.e. independent of specimen size, if this energy is calculated correctly and completely [16,22,23]. In this study on SFRC due to presence of fibers and consequently other energy consumption factors, measured fracture energy values are more scattered. The fibers orientation and embedment length in the crack front affect fracture energy. For SFRC beams, more samples and larger sizes could yield better results. In Figure 13, it is observed that, the increase in the offset ratio, increases G_F values. This is again a result of mixed mode condition. It seems that energy dissipation due to friction and aggregate interlock increases the work of fracture. The average fracture energy for our study was 3.13 kJ/m^2, which is comparable to other studies [12,24]. If only the center notched beams are considered, the value of G_F = 2.98 kJ/m^2 will result. Fracture energy was also calculated by the second method, using the difference between two load-displacement curves for different center notched specimens. To utilize this method, it is logical to use those specimens which result in larger difference between notch depths. Also, in an unnotched specimen, there exists some extraneous energy dissipation regarding the place of starter crack. Therefore, the specimens with a_0 = 30 and 90 mm were selected (Figure 14). The fracture energy calculated by this method was 2.63 kJ/m^2, which is comparable to the first method results.

4. CONCLUSIONS

The mixed mode fracture of one percent volume fraction SFRC beam specimens was investigated. It was observed that the main effect of fibers was in the post-peak region, in which a significant increase in ductility was present. The peak loads were not much different from those of plain concrete. Although the condition of plane strain was approximated, the apparent mixed mode fracture toughness values had a large scatter.

The experimental crack initiation angles for SFRC are more scattered and the crack path is more tortuous than in plain concrete. The crack angles increase with the increase in ratio of mode II to mode I conventional critical stress intensity factors. Fracture energy values showed relatively large scatter, too. Fracture energy was calculated by two methods for center notched specimens, in which the results were comparable to each other. The fiber inclination and the relatively small ligament size to fiber size ratio are responsible for the large scatter in results. Larger specimens and more samples are required to obtain more reliable results for SFRC. The LEFM based maximum principal stress criterion may be used for crack path determination, for low volume fraction SFRC, approximately.

5. ACKNOLEDGEMENT

This research has been conducted in the Materials and Structures Laboratory of Civil Engineering Department at Sharif University of Technology.

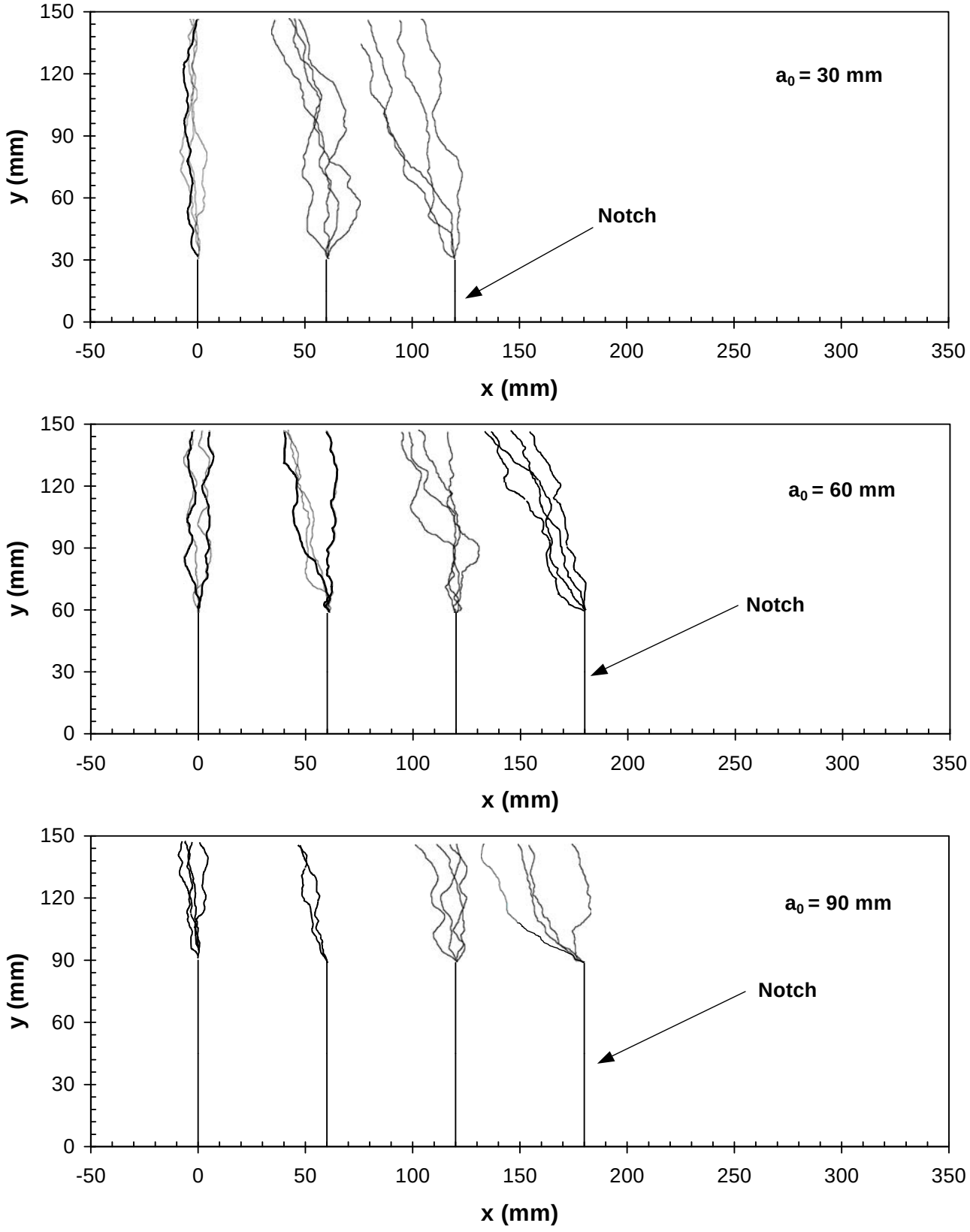

Figure 12. Crack trajectories for plain concrete (Kazemi, et al [20]).

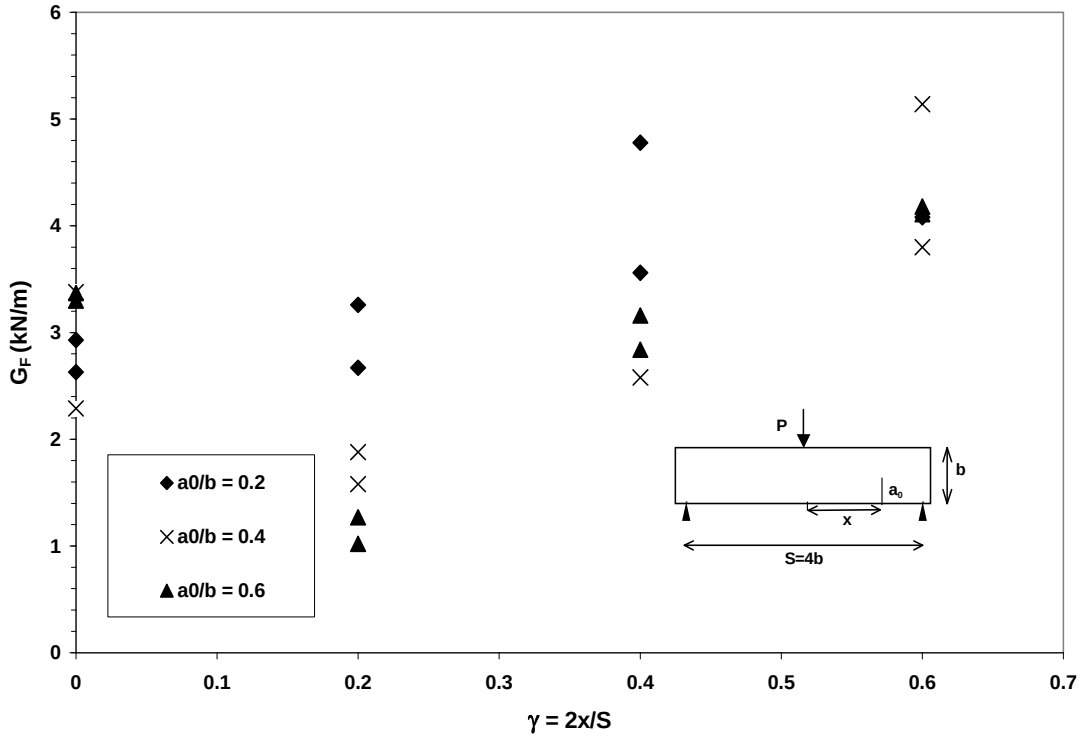

Figure 13. Variation of fracture energy with notch depth and location.

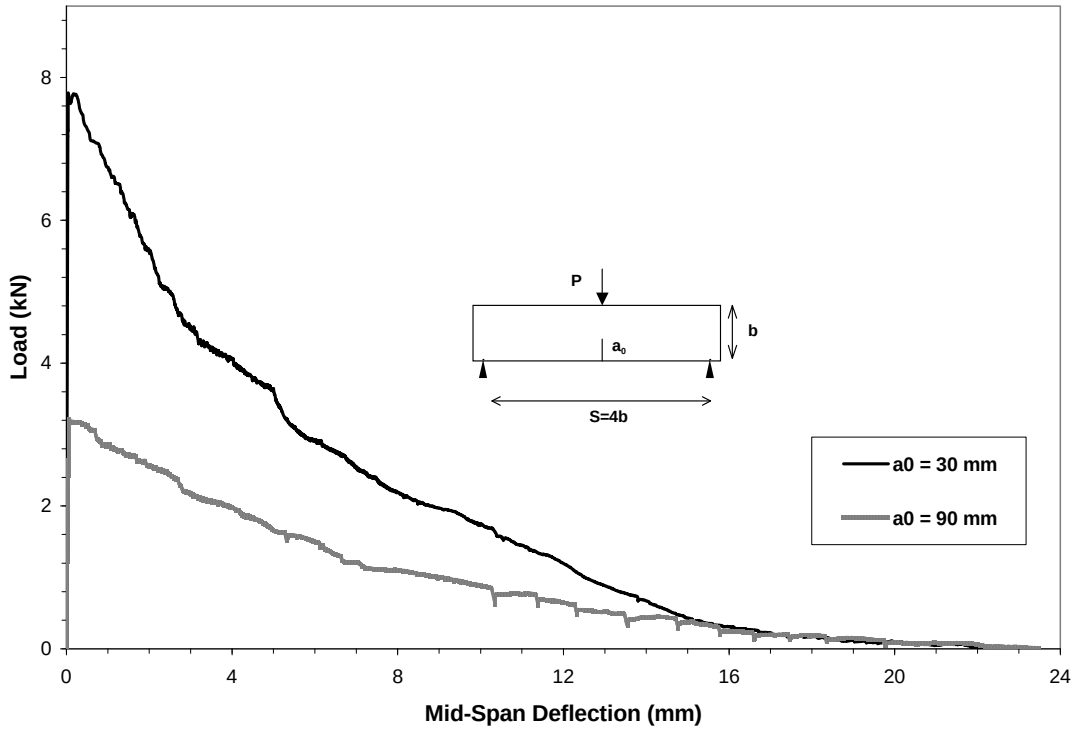

Figure 14. Load-deflection plots of two center notched beams with a_0 = 30 and 90 mm, for G_F calculation.

6. NOTATION

The following symbols are used in this paper:

a= Crack Depth
a_0= Notch Depth
b= Beam Depth
f'_c= Cylinder Compressive Strength
$f_I(\alpha,\gamma)$= Dimensionless Function for Mode I
$f_{II}(\alpha,\gamma)$= Dimensionless Function for Mode II
G_F= Fracture Energy
K_I= Mode I Stress Intensity Factor
K_{IC}= Mode I Fracture Toughness
K_{ICM}= Mode I Apparent Fracture Toughness in the Mixed Mode Condition
K_{II}= Mode II Stress Intensity Factor
K_{IIC}= Mode II Fracture Toughness
K_{IICM}= Mode II Apparent Fracture Toughness in the Mixed Mode Condition
L= Beam total length
M= Bending Moment at Distance x from the Beam's Centerline
M_0= Central Bending Moment of the Beam Generated by Dead Loads
P= Applied Load
P_0= An Equivalent Point Load Resulting in the Same Moment as the System of Dead Loads
R_1= Ratio of Work of Weight to Total Work of Fracture ($R_1 = W_W / W_F$)
R_2= Ratio of Work up to the Peak Load, to Total Work of Fracture ($R_2 = W_{P\max} / W_F$)
r= Ratio of K_{IICM} to K_{ICM}
S= Beam Span
t= Beam Thickness
u_0= Recorded Maximum Displacement when the Recorded Load Becomes Zero
V= Shear Force at Distance x from the Beam's Centerline
W_F= Total Work of Fracture
W_W= Work Done by the Self-Weigh of the Beam
w= Weight Per unit Length of the Beam
x= The Distance Between the Centerline of the Beam and the Place of Notch
α= Notch to Depth Ratio
γ= Offset Ratio
Δa= The Difference Between the Initial Notch Depths for Two Beams
θ= Crack Angle
θ_m= Crack Initiation Angle (Equation 3)
σ= A Stress Measure
σ_N= Nominal Tensile Stress (Equation 7)
σ_r, σ_θ= Normal Stress Components in Polar Coordinates (Figure 1)
τ_N= Nominal Shear Stress (Equation 8)
$\tau_{r\theta}$= Shear Stress Component (Figure 1)

7. REFERENCES

1. Balaguru, P.N. and Shah, S.P., "Fiber-Reinforced Cement Composites", McGraw-Hill, Singapore, (1992).
2. Carpinteri, A. and Massabo, R., "Reversal in Failure Scaling Transition of Fibrous Composites", ***ASCE J. Eng. Mech***., Vol. 123, No. 2, (1997), 107-114.
3. Mai, Y.W., "Cohesive Zone and Crack-Resistance (R)-Curve of Cementitious Materials and their Fiber-Reinforced Composites", ***Eng. Fracture Mech***., Vol. 69, (2002)., 219-234.
4. Jenq, Y.S. and Shah, S.P., "Crack Propagation in Fiber-Reinforced Concrete", ***ASCE J. Struct. Eng***., Vol. 112, No. 1, (1986), 19-34.
5. Shah, S.P., Swartz, S.E. and Ouyang, C., "Fracture Mechanics of Concrete", John Wiley, New York, U.S.A., (1995).
6. Banthia, N. and Sheng, J., "Fracture Toughness of Micro-Fiber Reinforced Cement Composites", ***Cement and Concrete Composites***, Vol. 18, (1996), 251-269.
7. Cotterell, B. and Mai, Y.W., "Fracture Mechanics of Cementitious Materials", Blackie Academic and Professional/Chapman and Hall, Glascow/London, U.K., (1996).
8. Biolzi, L., "Mixed Mode Fracture in Concrete Beams", ***Eng. Fracture Mech***., Vol. 35, (1990), 187-193.
9. Swartz, S.E. and Taha, N.M., "Mixed Mode Crack Propagation and Fracture in Concrete", ***Eng. Fracture Mech***., Vol. 35, (1990), 137-144.
10. Guo, Z.K., Kobayashi, A.S. and Hawkins, N.M., "Mixed Modes I and II Concrete Fracture: an Experimental Analysis", ***J. Ap. Mech***., Vol. 61, (1994), 815-821.
11. Galvez, J.C., Elices, M., Guinea, G.V. and Planas, J., "Mixed Mode Fracture of Concrete under Proportional and Nonproportional Loading", ***Inte. J. Fracture***, Vol. 94, (1998), 267-284.
12. Soroushian, P., Elyamany, H., Tlili, A. and Ostowari, K., "Mixed-Mode Fracture Properties of Concrete Reinforced with Low Volume Fractions of Steel and Polypropylene Fibers", ***Cement and Concrete Compos***., Vol. 20, (1998), 67-78.
13. Bazant, Z.P. and Planas, J., "Fracture and Size Effect in Concrete and other Quasibrittle Materials", CRC, Florida, U.S.A., (1997).
14. Jenq, Y.S. and Shah, S.P. "Mixed-Mode Fracture of Concrete", ***Inte. J. Fracture***, Vol. 38, (1988), 123-142.
15. ACI, "Guide for Specifying, Proportioning, Mixing,

Placing, and Finishing Steel Fiber Reinforced Concrete", ACI Committee 544, ACI 544.3R-93, 7, (1993).
16. Elices, M., Guinea, G. V. and Planas, J., "Measurement of the Fracture Energy Using Three-Point Bend Tests: Part 3-Influence of Cutting the P-δ Tail", ***Mat. Struct***., Vol. 25, (1992), 327-334.
17. Bazant, Z.P., "Concrete Fracture Models: Testing and Practice", ***Eng. Fracture Mech***., Vol. 69, (2002), 165-205.
18. Kazemi, M. T., Naraghi, M. and Vossoughi Shahvari, F., "Fracture Energy Determination of SFRC from Notched Beam Tests", 6th International RILEM Symposium on FRC-BEFIB, Vernna, Italy, (2004), 359-368.
19. ASTM, "Standard Test Method for Flexural Toughness and First-Crack Strength of Fiber-Reinforced Concrete (Using Beam with Third-Point Loading)", C1018, Philadelphia, (1998), 506-513.
20. Kazemi, M.T. and Vossoughi Shahvari, F., "Mixed Mode Fracture of Concrete: an Experimental Investigation", ***International Journal of Science and Technology***, Vol. 11, No. 4, (2004), 378-385.
21. Wollrab, E., Ouyang, C., Shah, S.P., Hamms, J. and Konig, G., "The Effect of Specimen Thickness on Fracture Behavior of Concrete", ***Magazine of Concrete Research***, Vol. 48, No.175, (1996), 117-129.
22. Jueshi, Q. and Hui, L., "Size Effect on Fracture Energy of Concrete Determined by Three-Point Bending", ***Cement and Concrete Research***, Vol. 27, No.7, (1997), 1031-1036.
23. Navalurkar, R.K., Hsu, C.T.T., Kim, S.K. and Wecharatana, M., "True Fracture Energy of Concrete", ***ACI Mat. J***., Vol. 96, No. 2, (1999), 213-225.
24. Kurihara, N., Kunieda, M., Kamada, T., Uchida, Y. and Rokugo, K., "Tension Softening Diagrams and Evaluation of Properties of Steel Fiber Reinforced Concrete", ***Eng. Fracture Mech***., Vol. 65, (2000), 235-245.